Journal of Solid State Chemistry **150,** 221–227 (2000)
doi:10.1006/jssc.1999.8589, available online at http://www.idealibrary.com on IDEAL®

Structure and Thermoelectric Transport Properties of Isoelectronically Substituted $(ZnO)_5In_2O_3$

Yoshitake Masuda,*,[1] Mitsuru Ohta,* Won-Seon Seo,* Wolfram Pitschke,† and Kunihito Koumoto*

*Department of Applied Chemistry, Graduate School of Engineering, Nagoya University, Furo-cho Chikusa-ku, Nagoya 464-8603, Japan; and †Institute of Solid State and Materials Research Dresden, Dresden D-01171, Germany

Received June 17, 1999; in revised form October 25, 1999; accepted November 22, 1999

We have proposed that homologous compounds of $(ZnO)_m In_2O_3$ with layer structures can become candidate materials for high-temperature thermoelectric conversion due to their low thermal conductivity and high electron mobility. Crystal structures can be modified by the isoelectronic substitution of either divalent or trivalent metal ions for Zn or In ions, respectively. Substitution of Mg^{2+}, Co^{2+}, and Y^{3+} gave rise to shrinkage of the *c* axis and elongation of the *a* axis of a hexagonal unit cell. Rietveld structure refinement indicated that Mg^{2+} and Co^{2+} ions occupy both 3*a* and 6*c* sites, while Y^{3+} ions occupy only 3*a* sites. An optimum amount of substitution of these cations increased electron mobility and hence thermoelectric efficiency $Z = \sigma\alpha^2/\kappa$ (σ = electrical conductivity, α = Seebeck coefficient, κ = thermal conductivity). *Z* values coupled with lowered thermal conductivity, which was possibly caused by suitable modification of the electronic structure, were associated with distortion of the crystal structure. For instance, the figure of merit of $(ZnO)_5(In_{0.97}Y_{0.03})_2O_3$ was $Z = 1.3\times10^{-4}$ K^{-1}. © 2000 Academic Press

Key Words: **crystal structure; Rietveld refinement; thermoelectric properties; zinc oxide; indium oxide; homologous series.**

INTRODUCTION

The homologous compounds $(ZnO)_mIn_2O_3$ (m = integer) show interesting properties suitable for specialized applications as a result of changes in the physical properties obtained by controlling the composition of materials composed of binary compounds. Minami *et al.* (1, 2) and the present authors (3) reported that ZnO–In_2O_3 films prepared by means of rf magnetron sputtering are promising as transparent electrodes for solar cells and flat panel displays. Because of their high thermal stability and rather high electrical conductivity they should be advantageous for high-temperature thermoelectric applications (4,5). Kazeoka *et al.* (6) tried to improve the thermoelectric transport properties of $(ZnO)_mIn_2O_3$ by partially substituting Y for In, and observed unusual behaviors of the thermoelectric transport properties: carrier density exhibited its minimum at $x = 0.03$ in $(ZnO)_5(In_{1-x}Y_x)_2O_3$, while the Seebeck coefficient and Hall mobility exhibited their maximum values. This was considered to be closely associated with the crystal structure of the compound.

Kasper (7) originally prepared $(ZnO)_mIn_2O_3$ (m = 2–5 and 7) and characterized it by recording X-ray powder diffraction patterns. Cannard and Tilley (8) analyzed $(ZnO)_mIn_2O_3$ (m = 4–5, 9, and 11) by high-resolution electron microscopy, and concluded that their structures were composed of metal–oxygen layers stacked perpendicular to the *c* axis of the hexagonal crystal system having the space group $R\bar{3}m$ for m = odd or $P6/3\,mmc$ for m = even. Kimizuka *et al.* (9) synthesized single crystals of $(ZnO)_mIn_2O_3$ (m = 3, 4, and 5) and took their Weissenberg photographs. They concluded $(ZnO)_mIn_2O_3$ to be isostructural with $(ZnO)_mLuFeO_3$ whose crystal structure had been determined by Isobe *et al* (10) from m = 1, 4, 5, and 6 using a single-crystal X-ray diffraction technique.

We (11) already investigated the structures of $(ZnO)_5In_2O_3$ and $(ZnO)_5(In_{0.8}Y_{0.2})_2O_3$ using the Rietveld refinement technique on the basis of the space group $R\bar{3}m$. The basic structure was found to consist of InO_2^- and $(InZn_5)O_6^+$ layers alternately stacked along the *c* axis. Y^{3+} ions were determined to occupy 3*a* sites substituting for In^{3+} ions. Appropriate lattice distortion introduced by elemental substitution was thought to cause a great change in the electronic structure and hence the conduction behavior. We tried to improve the thermoelectric transport properties of $(ZnO)_5In_2O_3$ by substituting Mg or Co ions for Zn ions and Fe or Y ions for In ions. We further studied their crystal structures using a Rietveld method to clarify the relationship between their thermoelectric properties and crystal structure.

EXPERIMENTAL

Sample Preparation

Starting powders of ZnO, In_2O_3, Y_2O_3, Fe_2O_3 (all 99.99% pure) and CoO and MgO (99.9% pure) were

[1] To whom correspondence should be addressed. Fax: +81-52-789-3201. E-mail: h981202d@mbox.media.nagoya-u.ac.jp.

0022-4596/00 $35.00

weighed in specific proportions to obtain the compositions given in Table 1 and were mixed in a ball mill for 24 h using zirconia balls and ethanol. The mixed powders were dried and heated at 1423 K for 6 h in air. After having been cooled, they were crushed in the ball mill again for 24 h. The powders were dried and pressed into compacts under the isostatic pressure of 196 MPa, and then sintered at 1823 K for 2 h in air.

X-Ray Diffraction Measurements

For X-ray diffraction measurements samples were pulverized in an agate mortar and pestle. Measurements were carried out with a Philips goniometer PW1820 equipped with a sample spinner, secondary graphite monochromator, and automatic divergence slit using Co$K\alpha$ radiation, and Cu$K\alpha$ radiation for the Co-substituted compounds. X-Ray diffraction diagrams were recorded in Bragg–Brentano geometry from $4^\circ(2\theta)$ to $130^\circ(2\theta)$ with steps of $0.03^\circ(2\theta)$. Measuring time was 10 s per step. Polycrystalline silicon was used for instrumental calibration. Observed diffraction pattern differed from that of the undoped compound. $(ZnO)_5In_2O_3$ (11), in reflection positions and intensities. They proved to consist of a single phase only.

Rietveld Refinement

For the Rietveld structure refinement we used the PC-RIETVELD PLUS program (Philips) (12). The refinement was started using the structure data of the undoped compound $(ZnO)_5In_2O_3$ (11). Afterward the *Me* ions were located at Zn^{2+} and In^{3+} sites, respectively, with *Me* = Y, Mg, Co, Fe. The pseudo-Voigt function was used for simulation of the peak shapes (13). Intensities within five times of the full width at half-maximum (FWHM) were considered to contribute to the reflection. Peaks below $42.5^\circ(2\theta)$ were corrected for asymmetry effects after Rietveld (14). The analysis of powder patterns resulted in a small preferred orientation effect along [001], which was corrected using the March model (15). The background as modeled by linear interpolation between 29 operator-selected points. At the first step, scaling factor, lattice constants, profile parameters, preferred orientation parameter, and atomic coordinates were refined. The diffraction patterns of metal-substituted compounds differed only slightly from that of an undoped compound. As a result, the occupation numbers of *Me* atoms allowed large standard deviation. For that reason the chemical composition was used as a constant in the refinement procedure. As observed in earlier studies (11) the occupation numbers of metal atoms correlate strongly, making their independent refinement impossible. Consequently, they were located arbitrarily at the metal sites *M*(1), *M*(2), *M*(3), and *M*(4), and the composition based on the resulting *R* values permitted us to determine the arrangement of atoms in the unit cell.

TABLE 1

No.		*Me* (Mg, Co, Fe)	Y	Zn	In	O
	$(ZnO)_5In_2O_3$	—	—	0.333	0.133	0.533[a]
	$(ZnO)_5(In_{0.8}Y_{0.2})_2O_3$	—	0.027	0.333	0.107	0.533[a]
1	$(Zn_{0.9}Mg_{0.1}O)_5In_2O_3$	0.033	—	0.300	0.133	0.533
2	$(Zn_{0.95}Mg_{0.05}O)_5In_2O_3$	0.017	—	0.317	0.133	0.533
3	$(Zn_{0.9}Co_{0.1}O)_5In_2O_3$	0.033	—	0.300	0.133	0.533
4	$(Zn_{0.95}Co_{0.05}O)_5In_2O_3$	0.017	—	0.317	0.133	0.533
5	$(ZnO)_5(In_{0.9}Fe_{0.1})_2O_3$	0.013	—	0.333	0.120	0.533
6	$(ZnO)_5In_{0.95}Fe_{0.05})_2O_3$	0.007	—	0.333	0.127	0.533
7	$(Zn_{0.9}Mg_{0.1}O)_5(In_{0.8}Y_{0.2})_2O_3$	0.033	0.027	0.300	0.107	0.533
8	$(Zn_{0.9}Co_{0.1}O)_5(In_{0.8}Y_{0.2})_2O_3$	0.033	0.027	0.300	0.107	0.533

[a] See (11).

TABLE 2

M(1)	0.08 (1)	0.08 (1)	0.08 (1)	0.08 (1)
M(2)	0.07 (1)	0.21 (1)	0.00 (1)	0.00 (1)
M(3)	0.07 (1)	0.00 (1)	0.21 (1)	0.00 (1)
M(4)	0.07 (1)	0.00 (1)	0.00 (1)	0.21 (1)
wR_p	7.73	9.37	8.60	9.89
R_B	5.35	6.51	6.30	7.63
M(1)	0.08 (1)	0.08 (1)	0.08 (1)	
M(2)	0.105 (1)	0.105 (1)	0.00 (1)	
M(3)	0.105 (1)	0.00 (1)	0.105 (1)	
M(4)	0.00 (1)	0.105 (1)	0.105 (1)	
wR_p	8.44	8.21	7.93	
R_B	5.94	6.14	5.81	

Table 2 gives the site occupancies and resulting *R* values for $(Zn_{0.9}Mg_{0.1}O)_5In_2O_3$. From this we can conclude the arrangement of the atoms with the same occupancies at all three 6*c* sites, which was proved to be realized for the other compounds investigated also. Due to a small atomic scattering factor of oxide ions in comparison with metal ions, refinement of oxygen occupation numbers has produced different solutions. Therefore, they were fixed without assuming any vacancies. Further details and the refined structure parameters are given in Tables 3A, 3B, and 4.

Measurements of Thermoelectric Properties

The specimens for thermoelectric measurements were cut out of the sintered bodies into rectangular bars of $5 \times 5 \times 15$ mm with a diamond saw. Heads of the two Pt–Pt 13% Rh thermocouples were embedded in the drilled holes at the ends of a specimen and fixed with platinum wires. Electrical conductivity was measured at 773–1123 K by a dc four-probe technique using each Pt leg of the thermocouple as a current lead. Two more Pt leads wound around the specimen were used to measure the voltage drop. For

TABLE 3A

		$(ZnO)_5In_2O_3$[b]		$(ZnO)_5(In_{0.8}Y_{0.2})_2O_3$[b]		$(Zn_{0.9}Mg_{0.1}O)_5In_2O_3$		$(Zn_{0.95}Mg_{0.05}O)_5In_2O_3$	
a (Å)		3.3285(1)		3.3505(1)		3.3318(1)		3.3300(1)	
c (Å)		58.127(2)		57.863(1)		57.950(2)		58.040(2)	
V (Å)^3		557.71(3)		562.53(2)		557.10(3)		557.39(3)	
d_x (g/cm^3)		6.11		5.97		5.94		6.02	
R_p (%)[a]		8.42		7.13		5.90		5.57	
wR_p (%)		10.52		9.05		7.73		7.30	
R_B (%)		8.56		6.94		5.35		5.06	
Atom	Site	Z	B (Å^2)	Z	B (Å^2)	Z	B (Å^2)	Z	B (Å^2)
M(1)	3a	0	1.1(1)	0	1.9(2)	0	0.9(1)	0	0.7(1)
M(2)Zn	6c	0.1894(1)	1.7(2)	0.1893(1)	2.7(2)	0.1899(1)	0.9(1)	0.1899(1)	0.8(1)
M(3)Zn	6c	0.0986(1)	1.9(2)	0.0989(1)	2.7(2)	0.0978(1)	1.0(1)	0.0976(1)	0.8(2)
M(4)Zn	6c	0.2804(1)	1.7(2)	0.2798(1)	2.9(2)	0.2809(1)	1.2(1)	0.2807(2)	1.6(2)
O(1)	6c	0.1464(2)	1.7(3)	0.1456(2)	2.8(3)	0.1468(2)	1.7(1)	0.1468(2)	1.4(2)
O(2)	6c	0.2286(3)	1.7(3)	0.2301(3)	2.8(3)	0.2281(2)	1.7(1)	0.2284(2)	1.4(2)
O(3)	6c	0.0629(3)	1.7(3)	0.0614(3)	2.8(3)	0.0627(2)	1.7(1)	0.0631(2)	1.4(2)
O(4)	6c	0.3163(3)	1.7(3)	0.3169(3)	2.8(3)	0.3150(2)	1.7(1)	0.3147(2)	1.4(2)

[a] For the definition of R values see (16, 17).
[b] See (11).

thermopower measurement, the temperature gradient in the specimen was generated by passing cool air in an alumina protection tube placed near one end of the specimen. The temperature difference between the two ends was controlled to be 2–15 K by varying the flow rate of air. Thermopower measured as a function of temperature difference gave a straight line and the Seebeck coefficient was calculated from its slope. Carrier density and Hall mobility as functions of substituted ions, x, were obtained from the Hall effect measurement (van der Pauw method) carried out at room temperature. The temperature dependence of thermal conductivity for the sintered samples was measured by the usual laser flash method (4).

RESULTS AND DISCUSSION

Figure 1 gives the rhombohedral unit cell of $(ZnO)_5In_2O_3$ which has been shown to be the basic structure of the investigated compounds with Me ions (Me = Mg, Co, Fe, Y) to be located at metal sites M(1), M(2), M(3), and M(4),

TABLE 3B

		$(Zn_{0.9}Co_{0.1}O)_5In_2O_3$		$(Zn_{0.95}Co_{0.05}O)_5In_2O_3$		$(ZnO)_5(In_{0.9}Fe_{0.1})_2O_3$		$(ZnO)_5(In_{0.95}Fe_{0.05})_2O_3$	
a (Å)		3.3295(1)		3.3284(1)		3.3205(2)		3.3248(1)	
c (Å)		58.026(2)		58.066(3)		57.926(2)		58.034(2)	
V (Å)^3		557.07(5)		557.10(5)		553.09(4)		555.59(4)	
d_x (g/cm^3)		6.09		6.11		6.06		6.08	
R_p (%)[a]		6.48		6.61		6.41		598	
wR_p (%)		8.33		8.71		8.33		7.79	
R_B (%)		7.22		8.79		5.30		4.83	
Atom	Site	Z	B (Å^2)	Z	B (Å)	Z	B (Å^2)	Z	B (Å^2)
M(1)	3a	0	0.5(1)	0	0.7(1)	0	1.0(1)	0	0.9(1)
M(2)Zn	6c	0.1901(1)	0.5(1)	0.1901(2)	0.8(1)	0.1901(1)	1.4(1)	0.1901(1)	0.9(2)
M(3)Zn	6c	0.0974(1)	0.4(1)	0.0972(1)	0.4(1)	0.0974(1)	0.9(1)	0.0974(1)	0.7(2)
M(4)Zn	6c	0.2814(1)	0.6(1)	0.2812(2)	1.5(1)	0.2811(2)	2.0(2)	0.2812(2)	1.5(2)
O(1)	6c	0.1466(3)	1.2(1)	0.1470(3)	1.4(1)	0.1463(2)	2.1(2)	0.1462(2)	1.9(2)
O(2)	6c	0.2285(3)	1.2(1)	0.2287(3)	1.4(1)	0.2281(2)	2.1(2)	0.2284(2)	1.9(2)
O(3)	6c	0.0624(3)	1.2(1)	0.0622(3)	1.4(1)	0.0626(2)	2.1(2)	0.0625(2)	1.9(2)
O(4)	6c	0.3159(3)	1.2(1)	0.3156(3)	1.4(1)	0.3160(2)	2.1(2)	0.3157(2)	1.9(2)

TABLE 4

	$(ZnO)_5In_2O_3$[a]		$(ZnO)_5(In_{0.8}Y_{0.2})_2O_3$[a]		$(Zn_{0.9}Mg_{0.1}O)_5In_2O_3$		$(Zn_{0.95}Mg_{0.05}O)_5In_2O_3$		$(Zn_{0.9}Co_{0.1}O)_5In_2O_3$		$(Zn_{0.95}Co_{0.05}O)_5In_2O_3$	
	M(1)	*M*(2), *M*(3), *M*(4)	*M*(1)	*M*(2), *M*(3), *M*(4)	*M*(1)	*M*(2), *M*(3), *M*(4)	*M*(1)	*M*(2), *M*(3), *M*(4)	*M*(1)	*M*(2), *M*(3), *M*(4)	*M*(1)	*M*(2), *M*(3), *M*(4)
Me	—	—	0.42(1)	0.00(2)	0.08(1)	0.07(1)	0.06(1)	0.03(1)	0.08(1)	0.07(1)	0.09(1)	0.03(1)
In	1.00(1)	0.19(2)	0.58(1)	0.17(2)	0.92(1)	0.18(1)	0.94(1)	0.18(1)	0.92(1)	0.18(1)	0.91(1)	0.18(1)
Zn	0.00(1)	0.81(2)	0.00(1)	0.83(2)	0.00(1)	0.75(1)	0.00(1)	0.79(1)	0.00(1)	0.75(1)	0.01(1)	0.79(1)

	$(ZnO)_5(In_{0.9}Fe_{0.1})_2O_3$		$(ZnO)_5(In_{0.95}Fe_{0.05})_2O_3$		$(Zn_{0.9}Mg_{0.1}O)_5In_{0.8}Y_{0.2})_2O_3$		$(Zn_{0.9}Co_{0.1}O)_5(In_{0.8}Y_{0.2})_2O_3$	
	M(1)	*M*(2), *M*(3), *M*(4)	*M*(1)	*M*(2), *M*(3), *M*(4)	*M*(1)	*M*(2), *M*(3), *M*(4)	*M*(1)	*M*(2), *M*(3), *M*(4)
Me	0.15(1)	0.01(1)	0.10(1)	0.00(1)	0.04(1)	0.08(1)	0.07(1)	0.07(1)
Y	—	—	—	—	0.42(1)	0.00(1)	0.42(1)	0.00(1)
In	0.85(1)	0.17(1)	0.90(1)	0.18(1)	0.54(1)	0.17(1)	0.51(1)	0.18(1)
Zn	0.00(1)	0.82(1)	0.00(1)	0.82(1)	0.00(1)	0.75(1)	0.00(1)	0.75(1)

[a] See (11).

respectively (see Table 5). Mg^{2+} and Co^{2+} ions were determined to be arranged at the 3*a*[*M*(1)] and 6*c*[*M*(2), *M*(3), *M*(4)] sites substituting for Zn^{2+} ions, while Y^{3+} and Fe^{3+} ions occupy 3*a* sites only substituting for In^{3+} ions. In the case of Mg- and Co-doped compounds site occupancies at *M*(1) are almost fixed even if fractions of substituted ions are changed, but those of *M*(2), *M*(3), and *M*(4) vary a lot with the change in the substituted fraction. Mg and Co ions are considered to easily occupy *M*(1) compared with other sites. In addition, *M*(2), *M*(3), and *M*(4) will be occupied when these ions can no longer enter *M*(1). The *M*(1) site occupancies of Co-substituted compounds are slightly larger than those of Mg-substituted compounds. Obviously Co ions more easily occupy *M*(1) than Mg ions. Fe-substituted compounds have been characterized by a larger quantity of Fe ions to be arranged at 3*a* [*M*(1)] sites possibly because of the smaller ionic radius of Fe^{3+} ions (550 pm) compared with those of Co^{2+} (650 pm), Mg^{2+} (720 pm), Zn^{2+} (740 pm), In^{3+} (810 pm), and Y^{3+} (920 pm) (18).

Figures 2 and 3 give the lattice constants and unit cell volume as derived from Rietveld refinement. Fe-substituted specimens shrank in both *a*-axis and *c*-axis directions with an increasing amount of substituted Fe because of its small ionic radius. In contrast, partial substitutions of Mg, Co, and Y all showed a common tendency in that the *a* axis expanded and the *c* axis shrank. The unit cell volumes of the Mg-, Co-, and Fe-substituted compounds were found to be smaller than that of the undoped compound because of their small ionic radii. In Table 5 are listed the distances between the metal oxide layers perpendicular to the *c* axis of the unit cell calculated on the basis of the atomic positions (see Table 3). As previously supposed by Kazeoka *et al.* (6) for Y-substituted compounds, octahedral voids of InO_2^- layers expand and tetrahedrons of $(InZn_5)O_6^+$ layers shrink along the *c* axis. In contrast in Co-, Mg-, and Fe-substituted compounds voids of InO_2^- layers shrink, whereas the interior tetrahedrons of $(InZn_5)O_6^+$ layers slightly expand.

TABLE 5

	$(ZnO)_5In_2O_3$	$(ZnO)_5(In_{0.8}Y_{0.2})_2O_3$	$(Zn_{0.9}Mg_{0.1}O)_5In_2O_3$	$(Zn_{0.9}Co_{0.1}O)_5In_2O_3$	$(ZnO)_5(In_{0.9}Fe_{0.1})_2O_3$
$(Me(2))_2O_2$	2.645	2.633	2.695	2.716	2.647
$(Me(2))_2O_2$	2.633	2.622	2.642	2.663	2.653
$(Me(3))_2O_2$	2.656	2.639	2.631	2.634	2.636
$(Me(4))_2O_2$	3.075	3.096	3.037	3.017	3.041
$Me(1)O_2$					

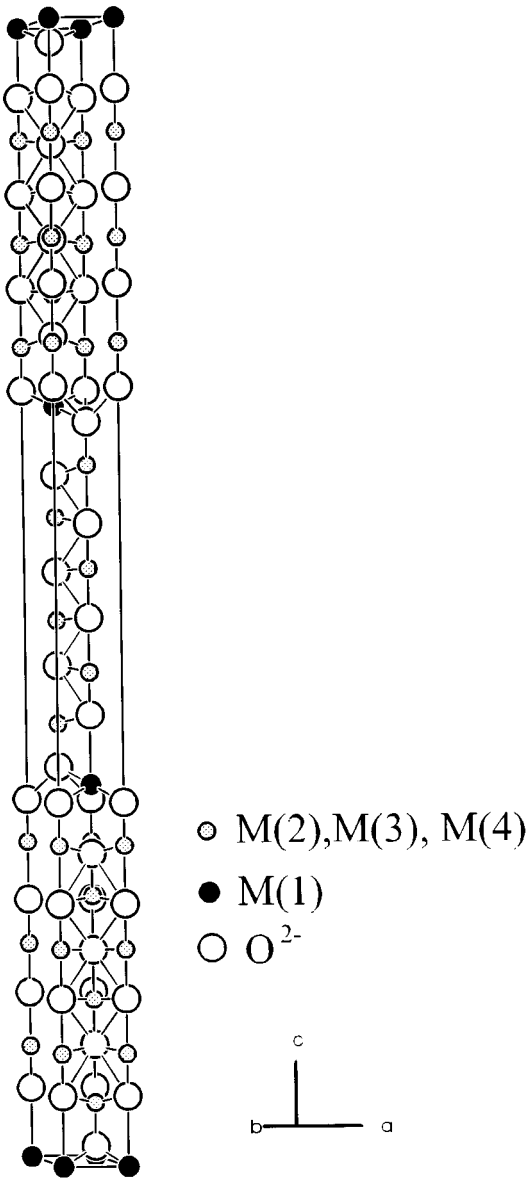

FIG. 1. Crystal structure of $(ZnO)_5In_2O_3$ as derived from Rietveld refinement (space group $R\bar{3}m$).

Temperature dependences of both electrical conductivity and Seebeck coefficient were observed to be all similar for substituted specimens, though their absolute values differed greatly depending on the kind of substituted ions. Figure 4 shows the Seebeck coefficient and electrical conductivity measured at 1073 K as a function of substituted ions, x. For all samples with $x > 0.05$ electrical conductivity decreased gradually with increasing amount of substituted ions in all cases investigated, which is obviously caused by electron scattering on an increase in the number of defects in crystal structure. Seebeck coefficients were always negative, hinting

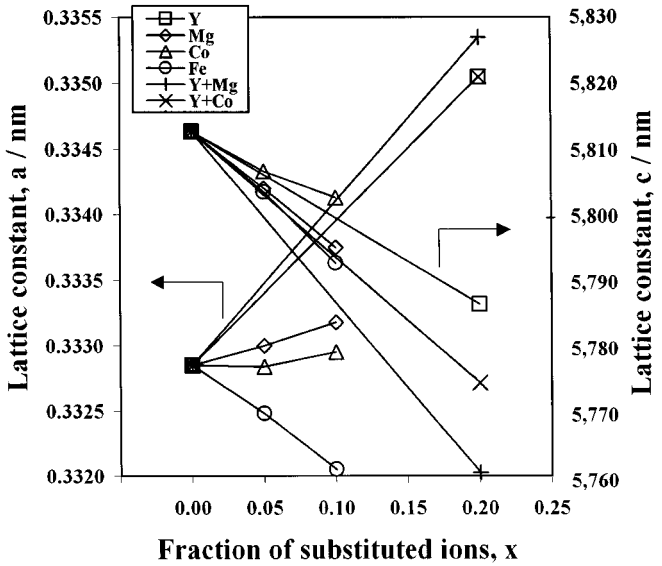

FIG. 2. Relationship between lattice constant and x for $(ZnO)_5(In_{1-x}Y_x)_2O_3$, $(ZnO_{1-x}Mg_x)_5In_2O_3$, $(Zn_{1-x}Co_x)_5In_2O_3$, $(ZnO)_5(In_{1-x}Fe_x)_2O_3$, $(Zn_{0.9}Mg_{0.1})_5(In_{1-x}Y_x)_2O_3$, and $(Zn_{0.9}Co_{0.1})_5(In_{1-x}Y_x)_2O_3$.

that the investigated compounds showed maxima at $x = 0.005$ and that of Y-substituted compounds at $x = 0.03$. On the other hand, Fe substitution gave rise to a decrease in the Seebeck coefficient with a minimum at $x = 0.01$. Accordingly, the power factor ($\sigma\alpha^2$) showed an extremum at corresponding x values (Fig. 5). Site occupancies of Mg and

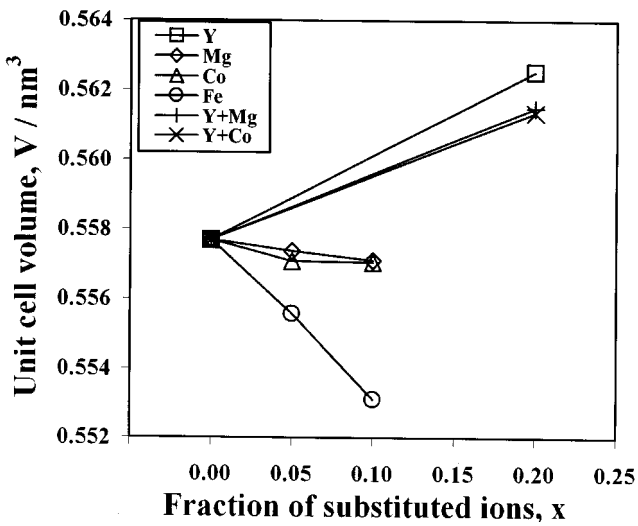

FIG. 3. Relationship between unit cell volume and x for $(ZnO)_5(In_{1-x}Y_x)_2O_3$, $(Zn_{1-x}Mg_x)_5In_2O_3$, $(Zn_{1-x}Co_x)_5In_2O_3$, $(ZnO)_5(In_{1-x}Fe_x)_2O_3$, $(Zn_{0.9}Mg_{0.1})_5(In_{1-x}Y_x)_2O_3$, and $(Zn_{0.9}Co_{0.1})_5(In_{1-x}Y_x)_2O_3$.

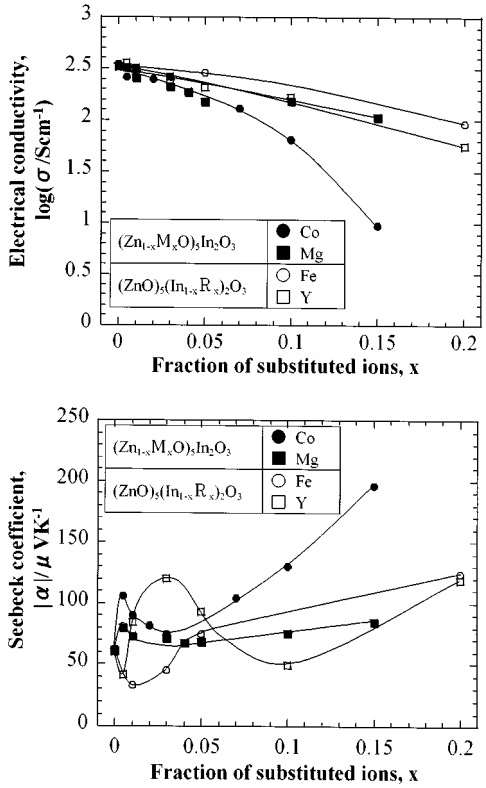

FIG. 4. Plots of electrical conductivity and Seebeck coefficient as functions of amount of substituted ions, x, at 1073 K.

Co at $M(1)$ become maximum (0.08) when the fraction of substituted ions is $x = 0.016$, and the falling gradient of power factor becomes gentle at this point ($x = 0.016$). Furthermore, the power factor reaches a maximum when metal ions occupy the $M(1)$ position only and when they occupy about one-third of the maximum site occupancies of metal atoms at $M(1)$. In the case of Y- and Co-substituted compounds the carrier density decreases with increasing amount of substituted ions showing an absolute minimum which coincides with the composition to give the largest power factor at high temperatures (Fig. 6). At the same time Hall mobility showed a maximum, which is the case for the Mg-doped compounds also. For the Fe-substituted compounds inverted behavior was observed. In general, the unusual behavior of thermoelectric transport properties is supposed to be caused by the site occupancy of metal ions at $M(1)$ sites and the changes in structure namely, distortion of crystal lattice giving rise to changed electronic structure and scattering behavior of carriers. However, a fundamental understanding of structure–property relations requires calculation of the electronic structure which would be useful also for the purpose of further improving the thermoelectric properties in this system through certain effective and appropriate partial substitutions. Figure 7 shows the temperature dependence of thermal conductivity for the sintered samples with the compositions $(ZnO)_5In_2O_3$, $(Zn_{0.995}Mg_{0.005}O)_5In_2O_3$, and $(ZnO)_5(In_{0.97}Y_{0.03})_2O_3$. As a result of structural disorder caused by substitution of Mg and Y ions the corresponding compounds showed thermal conductivity $\sim$60 and $\sim$30% lower than that of

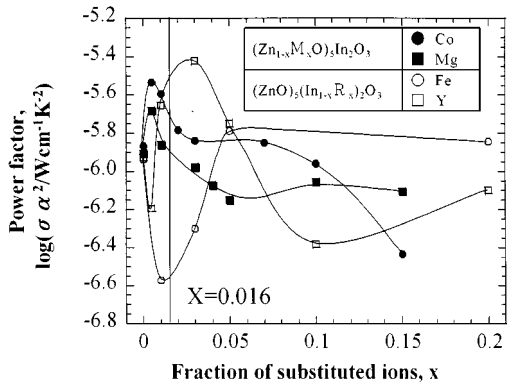

FIG. 5. Relationship between power factor and x for $(ZnO)_5(In_{1-x}Y_x)_2O_3$, $(Zn_{1-x}Mg_x)_5In_2O_3$, $(Zn_{1-x}Co_x)_5In_2O_3$, and $(ZnO)_5(In_{1-x}Fe_x)_2O_3$.

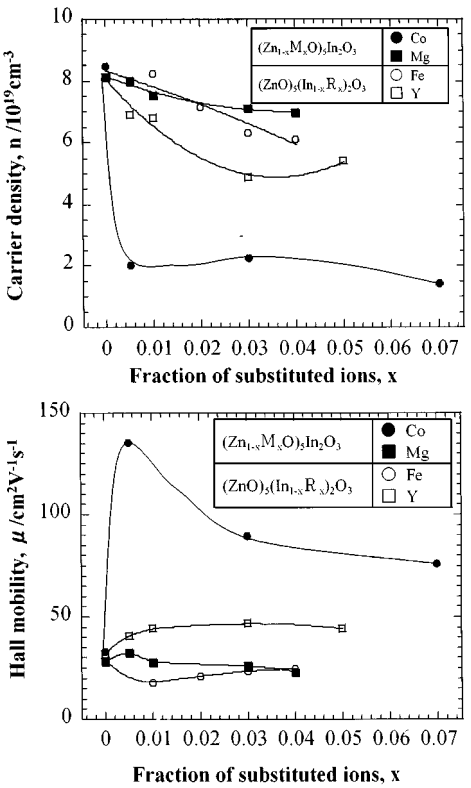

FIG. 6. Plots of carrier density and Hall mobility as functions of amount of substituted ions, x, at room temperature.

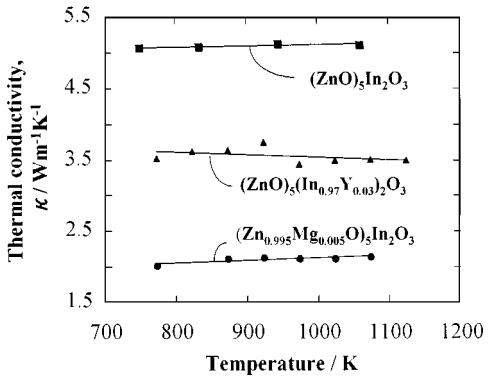

FIG. 7. Temperature dependence of thermal conductivity, κ, of the sintered samples with the compositions $(Zn_{0.995}Mg_{0.005}O)_5In_2O_3$, $(ZnO)_5(In_{0.97}Y_{0.03})_2O_3$, and $(ZnO)_5In_2O_3$.

an undoped compound. Consequently, the largest figure of merit obtained in this system was $Z = 1.3 \times 10^{-4}\ K^{-1}$ for $(ZnO)_5(In_{0.97}Y_{0.03})_2O_3$ (6). This value is substantially large compared with other *n*-type oxide materials. This system is considered to be one of the promising materials for the purpose of thermoelectric energy conversion (19). Hence for the purpose of improving the thermoelectric properties further in this system through certain effective and appropriate partial substitutions (i.e., expand to *a* axis and shrink to *c* axis), it is necessary to analyze the electronic structure–property relations associated with the site occupancies of substituted ions in the crystal lattice.

CONCLUSIONS

The crystal structure of isoelectronically substituted $(ZnO)_5In_2O_3$ compounds was analyzed using the Rietveld method. In addition the thermoelectric transport properties were measured as a function of substituted ions. The elemental substitution introduces an appropriate lattice distortion leading to a great change in conduction behavior. The unusual behavior of thermoelectric transport properties is supposed to be caused by the site occupancy of metal ions at *M*(1) sites. However, a detailed discussion of structure–property correlations in $(ZnO)_5In_2O_3$ requires calculation of the electronic structure.

ACKNOWLEDGMENTS

We thank Dr. Y. Yamauchi and Dr. K. Watari of the National Industrial Research Institute of Nagoya for their kind cooperation in the laser flash measurement of thermal conductivity. We are indebted to the Institute of Solid State and Materials Research Dresden for financial support of one of the authors (Y.M.) during his stay at the Institute of Solid State Analysis and Structural Research Dresden. We thank K. Stange and B. Opitz of the Institute of Solid State and Materials Research Dresden for their help in the XRD experiments.

REFERENCES

1. T. Minami, T. Kakumu, Y. Takeda, and S. Takata, *Thin Solid Films* **290,** 1 (1996).
2. T. Minami, T. Kakumu, Y. Takeda, and S. Takata, *J. Vac. Sci. Technol.* **14,** 1704 (1996).
3. H. Hiramatsu, W.-S. Seo, and K. Koumoto, *Chem. Mater.* **10,** 3033 (1998).
4. H. Ohta, W.-S. Seo, and K. Koumoto, *J. Am. Ceram. Soc.* **79,** 2193 (1996).
5. H. Hiramatsu, H. Ohta, W.-S. Seo, and K. Koumoto, *J. Jpn. Soc. Powder Powder Metall.* **44,** 44 (1997).
6. M. Kazeoka, H. Hiramatsu, W.-S. Seo, and K. Koumoto, *J. Mater. Res.* **13,** 523 (1998).
7. H. Kasper, *Z. Anorg. Allg. Chem.* **349,** 113 (1967).
8. P. J. Cannard and R. J. D. Tilley, *J. Solid State Chem.* **73,** 418 (1988).
9. N. Kimizuka, M. Isobe, and M. Nakamura, *J. Solid State Chem.* **116,** 170 (1995).
10. M. Isobe, N. Kimizuka, M. Nakamura, and T. Mohri, *Acta Crystallogr. Sect. C* **50,** 332 (1994).
11. W. Pitschke and K. Koumoto, *Powder Diffraction* (1998), **14,** 213 (1999).
12. PC-Rietveld plus Software Operation Manual Version 1.0, Philips Industrial Electronics B. V., The Netherlands, 1993.
13. R. A. Young and D. B. Wiles, *J. Appl. Crystallogr.* **15,** 430 (1982).
14. H. M. Rietveld, *J. Appl. Crystallogr.* **2,** 65 (1969).
15. W. A. Dollase, *Acta Crystallogr.* **19,** 267 (1986).
16. R. J. Hill and R. X. Fischer, *J. Appl. Crystallogr.* **23,** 462 (1990).
17. A. Young, E. Prince, and R. A. Sparks, *J. Appl. Crystallogr.* **15,** 357 (1982).
18. R. D. Shannon, *Acta Crystallogr. Sect. A* **32,** 751 (1976).
19. N. Murayama and K. Koumoto, *Ceramics* **33,** 161 (1998).